Supporting Information

Exploration of the electrochemical mechanism of ultrasmall multiple phases molybdenum carbides nanocrystals for hydrogen evolution reaction

Chunyong He*[a,b], Juzhou Tao*[a.b]

Dr. C. He, Prof. J. Tao

[a] Institute of High Energy Physics, Chinese Academy of Sciences (CAS), Beijing 100049, China

[b] Dongguan Neutron Science Center, Dongguan 523803, China

*e-mail: taoj@ihep.ac.cn (J. Tao); hechunyong@ihep.ac.cn

Experimental section

Chemicals and Reagents

Concentrated sulfuric acid (H_2SO_4, 98 wt%), potassium permanganate ($KMnO_4$), sodium nitrate ($NaNO_3$), hydrogen peroxide solution (30 wt%), ammonium molybdate ($(NH_4)_6Mo_7O_{24}\cdot 4H_2O$) and graphite powders (325 mesh, XFNANO Material Technologic Co. Ltd., Nanjing, China). Platinum on an XC-72 support (Pt/C, 20 wt%) was purchased and used as received (TKK, Japan).

Synthesis of graphite oxide (GO)

GO powders were synthesized via a modified Hummers method. In a typical process, 2.0 g natural graphite powders were gradually added into the concentrated H_2SO_4 (46 mL, 98 wt%) under stirring in an ice bath and the stirring continued for 15

min after mixing. Then 10.0 g $KMnO_4$ and 5.0 g $NaNO_3$ were slowly added in under vigorous agitation to keep the suspension temperature lower than 20 ^oC, before the temperature was raised to 40 ^oC and retained for 35 min. Afterwards, 50 ml of deionized water was added to the mixture slowly and the suspension temperature kept at 95 ^oC for 30 min. Finally 200 mL deionized water and 10 ml of 30% H_2O_2 were added into the suspension. At the end of the reaction, the color of the solution changed from dark brown to yellow. The mixture was filtered and washed with 1 $molL^{-1}$ HCl aqueous solution (250 mL) and deionized water to remove metal ions.

Growth of molybdenum carbides on graphene sheets

Typical procedure for preparing molybdenum carbides on graphene sheets (MoC-G and Mo_2C-G) is as follows. 0.8 g GO wad was first dissolved in 200 mL deionized water in a beaker sonicated for 2 h. 0.36g $(NH_4)_6Mo_7O_{24} \cdot 4H_2O$ was dissolved in 50 mL deionized water in a beaker, then the resulted solution poured into the GO suspension sonicated for 30 min. The mixture was dried at 90 ^oC until turning into hydrogel-like mixture then freeze dried. Further annealing in a tube furnace under Argon at 750-900 ^oC for 2 h forms molybdenum carbides. Ramping rate in tube furnace was controlled at 5 $°Cmin^{-1}$ and the final products were cooled down to 30 °C in the tube furnace at 10 $°Cmin^{-1}$. The annealing temperature is 750 °C for MoC-G and 900 °C for Mo_2C-G.

Characterizations

X-ray diffraction (XRD) was performed on a Rigaku D/Max-III using Cu Kα radiation operating at 30 kV and 30 mA. 2θ angular regions between 10° and 80° were measured at a scan rate of 6 $°min^{-1}$. X-ray photoelectron spectroscopy (XPS) measurements were carried out on an XPS apparatus (ESCALAB 250, Thermo-VG Scientific Ltd.). Transmission electron microscopy (TEM) and high-angle annular dark-field scanning transmission electron microscopy (HAADF-STEM) were performed on a field emission transmission electron microscope (FETEM, FEI Tecnai

G2 F30) operating at 300 kV. N_2 adsorption experiments using an ASAP 2020 Surface Area Analyzer (Micrometeritics Co., USA) were conducted to investigate sample porosity. All the samples were outgassed at 200 ^oC in a nitrogen flow for 4 h prior to the measurement. Nitrogen adsorption data were recorded at the liquid nitrogen temperature (77 K) and also used to calculate sample specific surface area using the Brunauer-Emmett-Teller (BET) equation in relative pressure between 0.014 and 0.2. Pore volumes were estimated as the liquid volume of N_2 adsorption at the relative pressure of 0.99. Pore size distribution was determined using the density functional theory (DFT) method. Mo *K*-edge X-ray absorption spectroscopy (XAS) of a Mo foil standard and catalyst samples were recorded in total electron yield transmission mode at the beamline BL14W1 of the Shanghai Synchrotron Radiation Facility (SSRF), China.

Electrochemical measurements.

All electrochemical measurements were conducted in a standard three-electrode cell using 0.5 $molL^{-1}$ H_2SO_4 as the electrolyte solution, a piece of graphite (10×1 cm^{-2}) as the counter electrode, a reversible hydrogen electrode (RHE) as the reference electrode, and a glassy carbon disk (A=0.196 cm^2) as the working electrode. Electrocatalytic HER activity of molybdenum carbides was investigated by depositing samples at a mass loading of ~0.8 mg cm^{-2} prepared as follows: 5.0 mg catalyst was first dispersed in 0.5 mL ethanol and 0.5 mL Nafion solution (0.05 wt %, DuPont, USA), the mixture ultrasonicated for an hour to form a well-dispersed ink; a certain amount of the ink was then transferred onto the glass carbon electrode surface and dried under infrared lamp for 5 min to obtain a catalyst thin film.

The HER experiments were conducted on an Autolab PGSTAT 302 (ECO Chemie, Netherlands) at 25 ^oC in a thermostatic water bath. Linear sweep voltammetry (LSV) tests were performed at 5 mVs^{-1} scan rate. Before the HER measurements, the electrodes were pre-treated by cycling the potential between -0.4 and +0.4 V at a sweep rate of 50 mVs^{-1} for 30 cycles to activate the catalysts, remove surface contamination and stabilize electrochemical current. Electrochemical impedance

spectroscopy (EIS) measurements were recorded at frequency range of 100 kHz to 100 mHz with modulation amplitude of 10 mV. Stability of the catalysts was studied by cycling the potential between -0.3 and 0.2 V at a sweep rate of 50 mVs^{-1} for 2,000 cycles. Long-term (20 h) stability was also tested at controlled potentials.

For comparison, 46.7wt% platinum on VC-72 catalyst (Pt/C from TKK, Japan) was measured under identical conditions, the loading is 12.5 μgcm^{-2} for Pt metal.

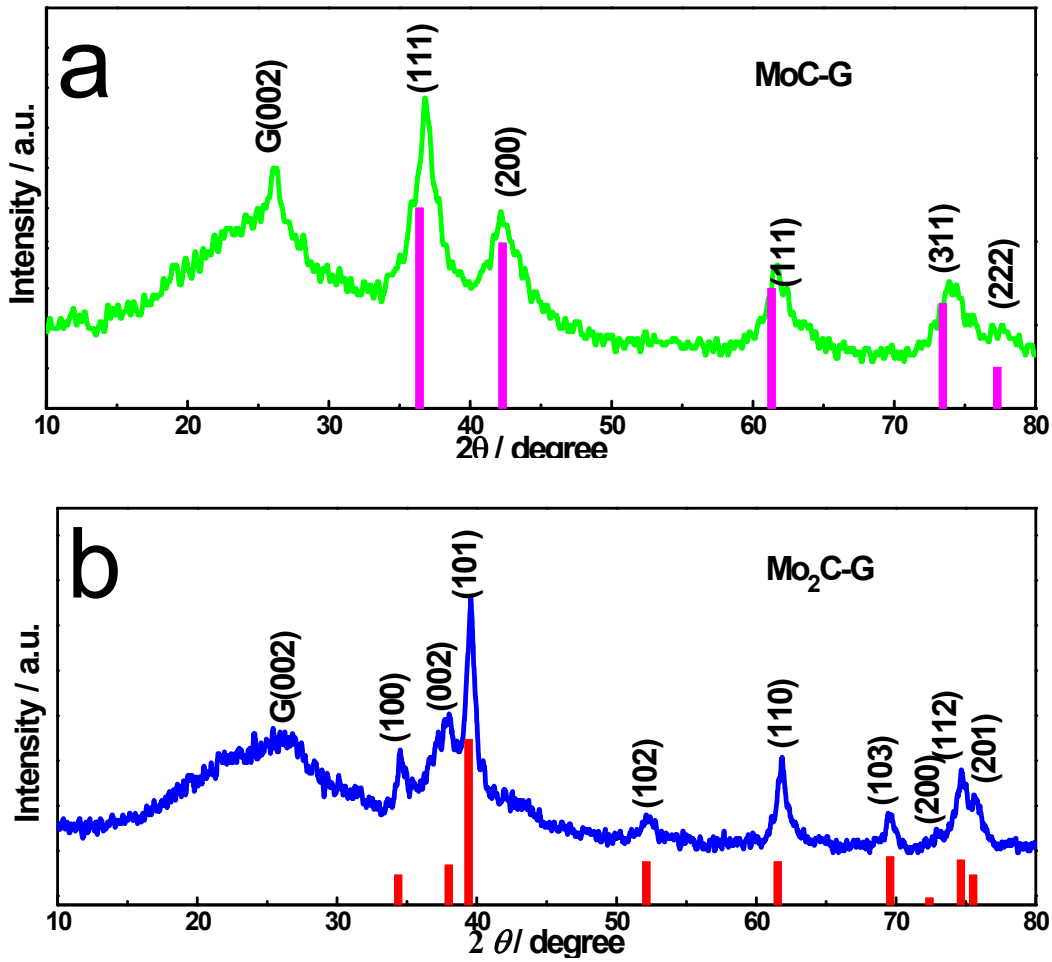

Figure S1 The XRD patterns of the ultrasmall molybdenum carbides nanocrystals on graphene support nanocomposites: (a) MoC-G and (b) Mo_2C-G.

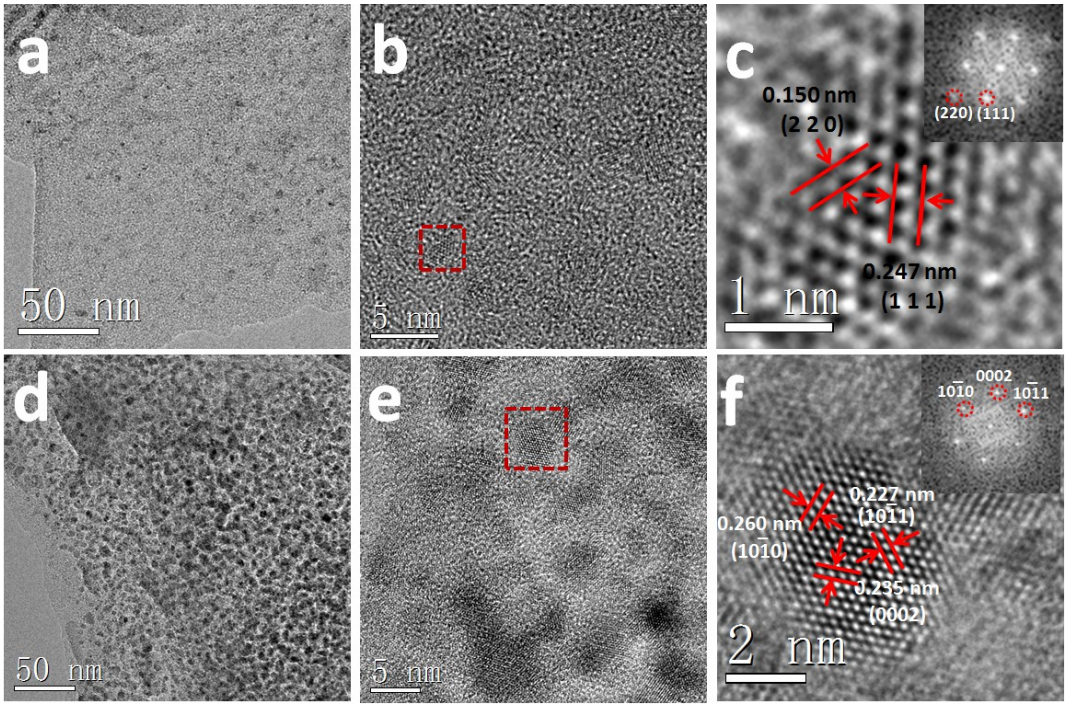

Figure S2 (a) TEM image of MoC-G, (b) HRTEM image of MoC-G, (c) close-up HRTEM image of the red square in (b), the inset is the corresponding fast Fourier transformation (FFT) pattern, (d) TEM image of Mo_2C-G, (e) HRTEM image of Mo_2C-G, (f) close-up HRTEM image of the red square in (e), the inset is the corresponding FFT pattern.

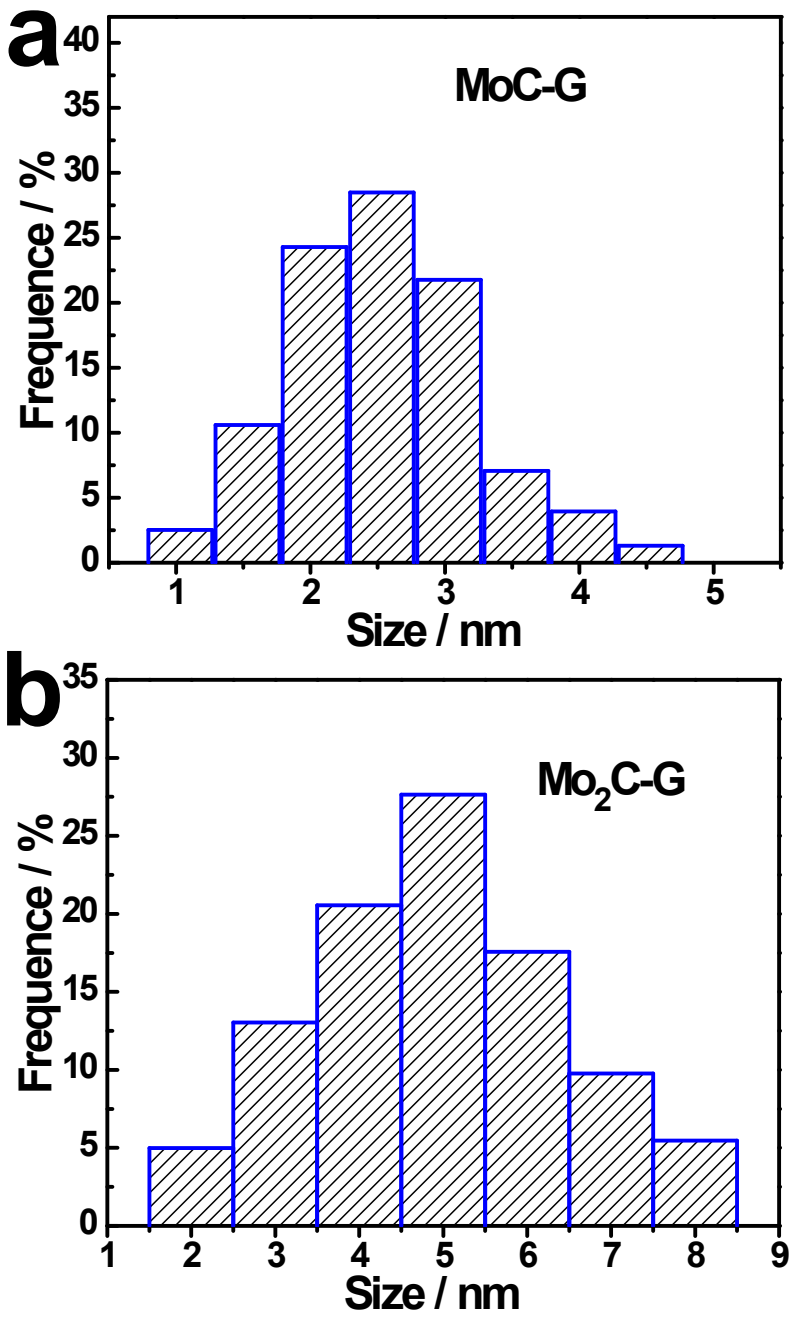

Figure S3 The size-distribution histograms of the (a) MoC-G and (b) Mo_2C-G.

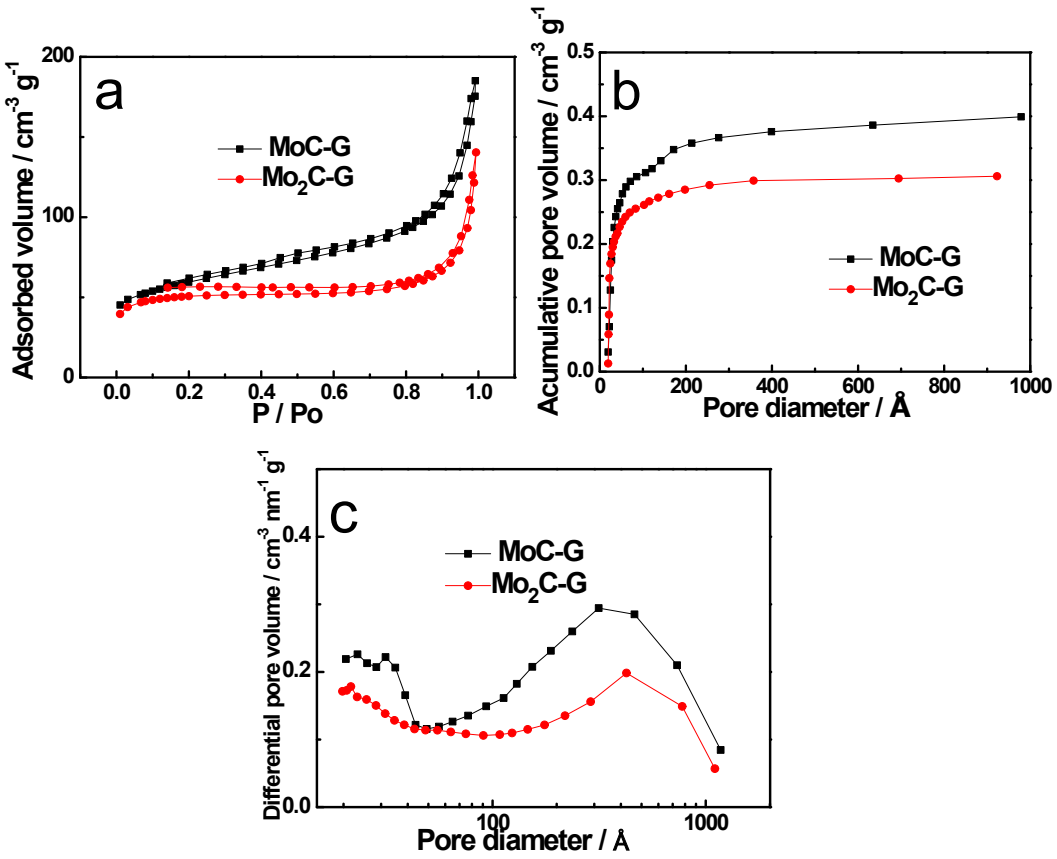

Figure S4 (a) Nitrogen adsorption/desorption isotherms of MoC-G and Mo_2C-G, (b) cumulative pore volumes of MoC-G and Mo_2C-G, (c) pore-size distribution curves of of MoC-G and Mo_2C-G.

Table S1. HER performance comparison of this work and recent reported other non-noble-metal HER electrocatalysts in acid media.

catalyst	electrolyte	E_0 / mV	η_{10} / mV	Loading / $mgcm^{-2}$	Tafel slope / $mVdec^{-1}$	j_0 / $mAcm^{-2}$	Refs
np-Mo_2C NW	0.5 $molL^{-1}$ H_2SO_4	/	130	0.21	53		[1]
Mo_2C/CNT	0.1 $molL^{-1}$ $HClO_4$	/	152	2	55.2	1.4×10^{-2}	[2]
Mo_2C/CNT-GR	0.5 $molL^{-1}$ H_2SO_4	-62	130	0.65	58	6.20×10^{-2}	[3]
Mo_2N/CNT-GR	0.5 $molL^{-1}$ H_2SO_4	-118	186	0.67	72	3.94×10^{-2}	[3]
MoS_2/CNT-GR	0.5 $molL^{-1}$ H_2SO_4	-140	255	0.65	100	2.91×10^{-2}	[3]
MoN/C	0.1 $molL^{-1}$ $HClO_4$	-157	>350	0.25	54.5	3.6×10^{-2}	[4]
NiMoN/C	0.1 $molL^{-1}$ $HClO_4$	-78	>250	0.25	35.9	0.24	[4]
Mo_2C-R	0.5 $molL^{-1}$ H_2SO_4	-68	~150	0.43	58	3.3×10^{-2}	[5]
Mo_2C	1 $molL^{-1}$ H_2SO_4	≥-100	~210	1.4	56	1.3×10^{-3}	[6]
MoB	1 $molL^{-1}$ H_2SO_4	≥-100	~210	2.5	55	1.4×10^{-3}	[6]
MoS_2/RGO	0.5 $molL^{-1}$ H_2SO_4	/	160	1	41	/	[7]
$[Mo_3S_{13}]^{2-}$	0.5 $molL^{-1}$ H_2SO_4	/	180	0.1	~40	/	[8]
CoP	0.5 $molL^{-1}$ H_2SO_4		85		50	0.2	[9]
MoP	0.5 $molL^{-1}$ H_2SO_4	-100	~200	0.36	56.4		[10]
CoSe	0.5 $molL^{-1}$ H_2SO_4		137	2.5-3	40	4.9×10^{-3}	[11]
MoC-G	0.5 $molL^{-1}$ H_2SO_4	~-30	221	0.8	88	2.55×10^{-2}	This wok
Mo_2C-G	0.5 $molL^{-1}$ H_2SO_4	~0	150	0.8	57	2.58×10^{-2}	This wok

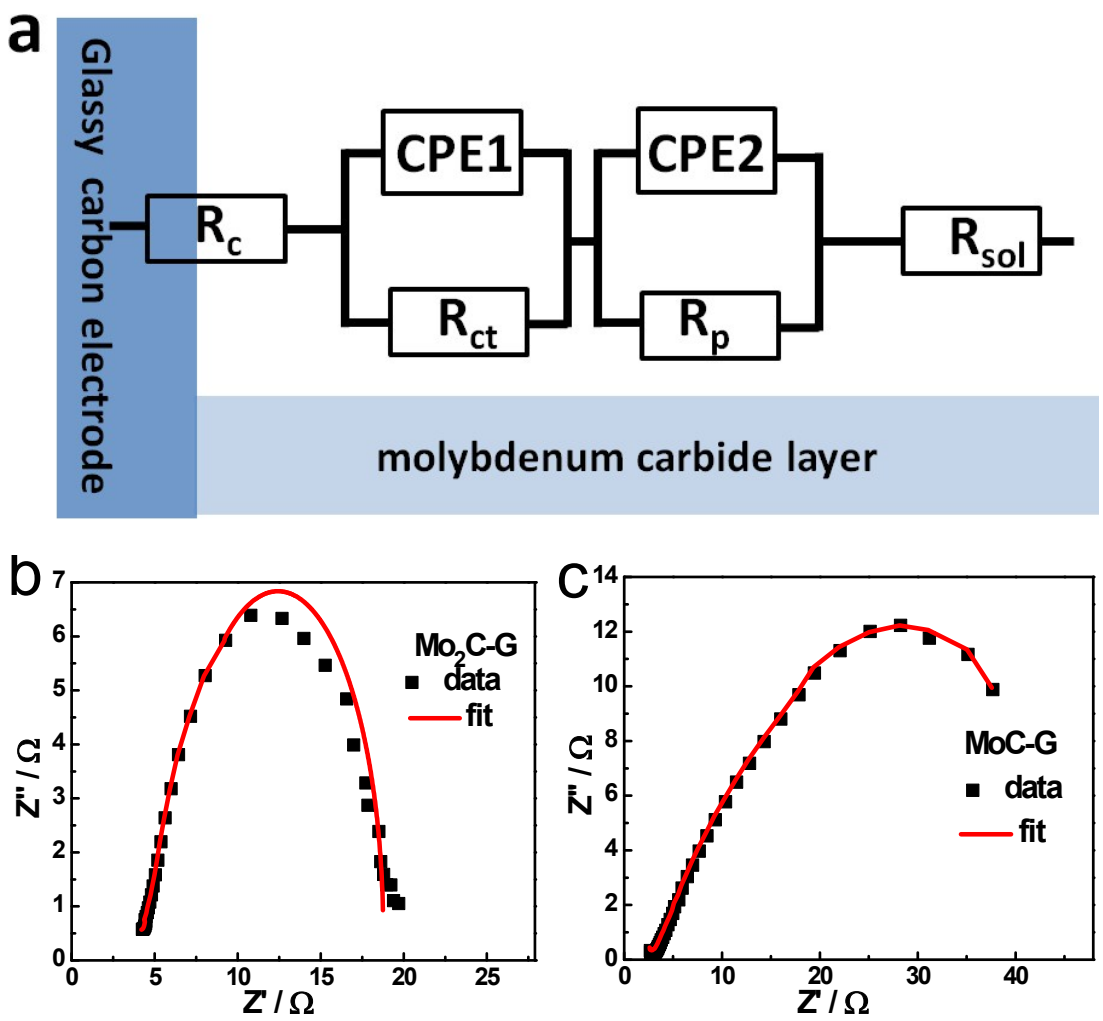

Figure S5 (a) The equivalent circuit for the impedance data using a transmission line model, where R_c represents the contact resistance of between the glassy carbon electrode and the catalyst layer, R_{sol} represents the solution resistance. In this model one branches is related to the charge-transfer process (C_{d1}-R_{ct}); another is related to the surface porosity (C_{d2}-R_p). The charge-transfer resistance R_{ct}, determined from the semicircle registered at low frequencies, reflects the HER kinetics, a smaller R_{ct} value corresponds to faster kinetics. The Nyquist plots of experimental and simulated data for (b) the Mo_2C-G and (c) the MoC-G catalysts simulated by the two-time-constant model.

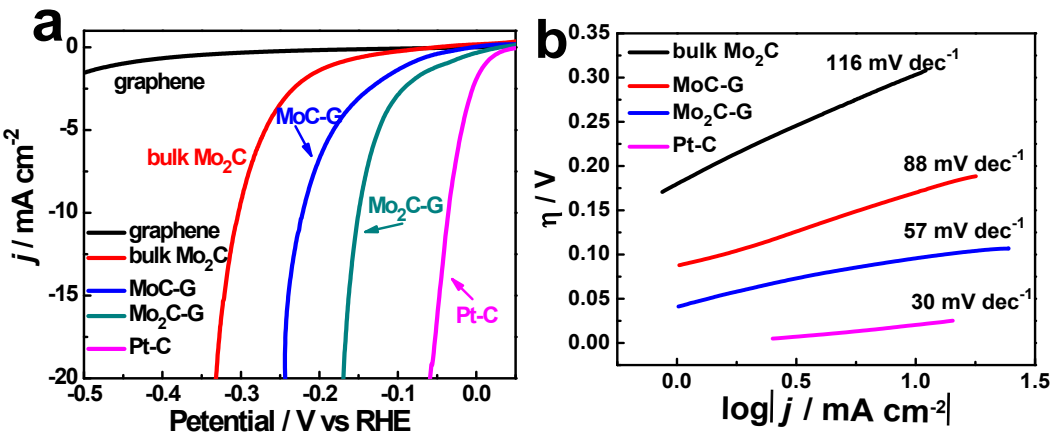

Figure S6 (a) Polarization curves of bulk Mo_2C, MoC-G, Mo_2C-G , Pt/C and graphene, (b) Tafel plots obtained from the polarization curves of various catalysts.

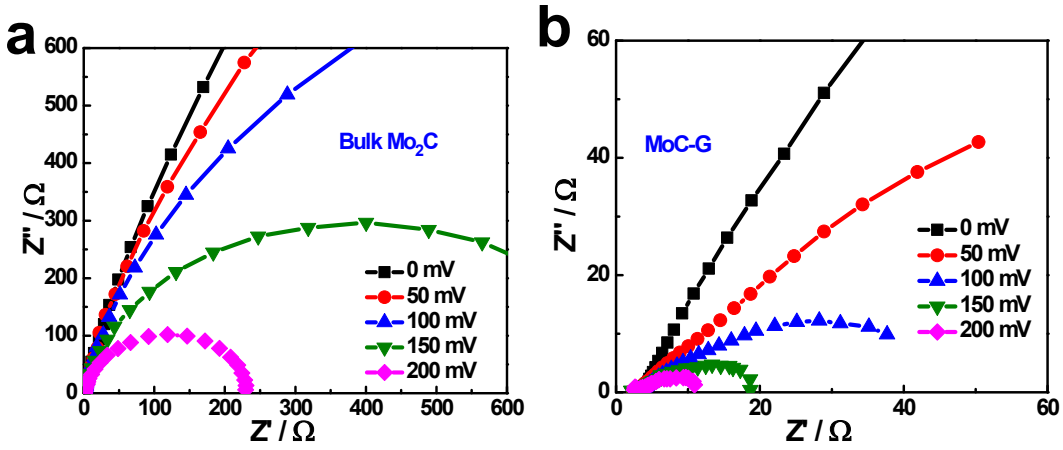

Figure S7 Nyquist plots showing EIS responses of bulk Mo_2C (a) and MoC-G (b) electrode at various HER overpotentials.

Table S2. Fit parameters from EIS for MoC-G and Mo_2C-G.

catalyst	η / mV	R_{sol} / Ω	R_c / Ω	R_{ct} / Ω	R_p / Ω
MoC-G	0	3.68	0.76	754.5	4.32
	50	3.95	0.76	145.5	4.32
	100	4.38	0.76	35.9	4.32
	150	4.59	0.76	9.8	4.32
	200	4.92	0.76	2.1	4.32
Mo_2C-G	0	4.69	0.84	633.4	3.86
	50	4.75	0.84	45.2	3.86
	100	4.83	0.84	10.4	3.86
	150	4.88	0.84	0.97	3.86
	200	4.97	0.84	0.32	3.86

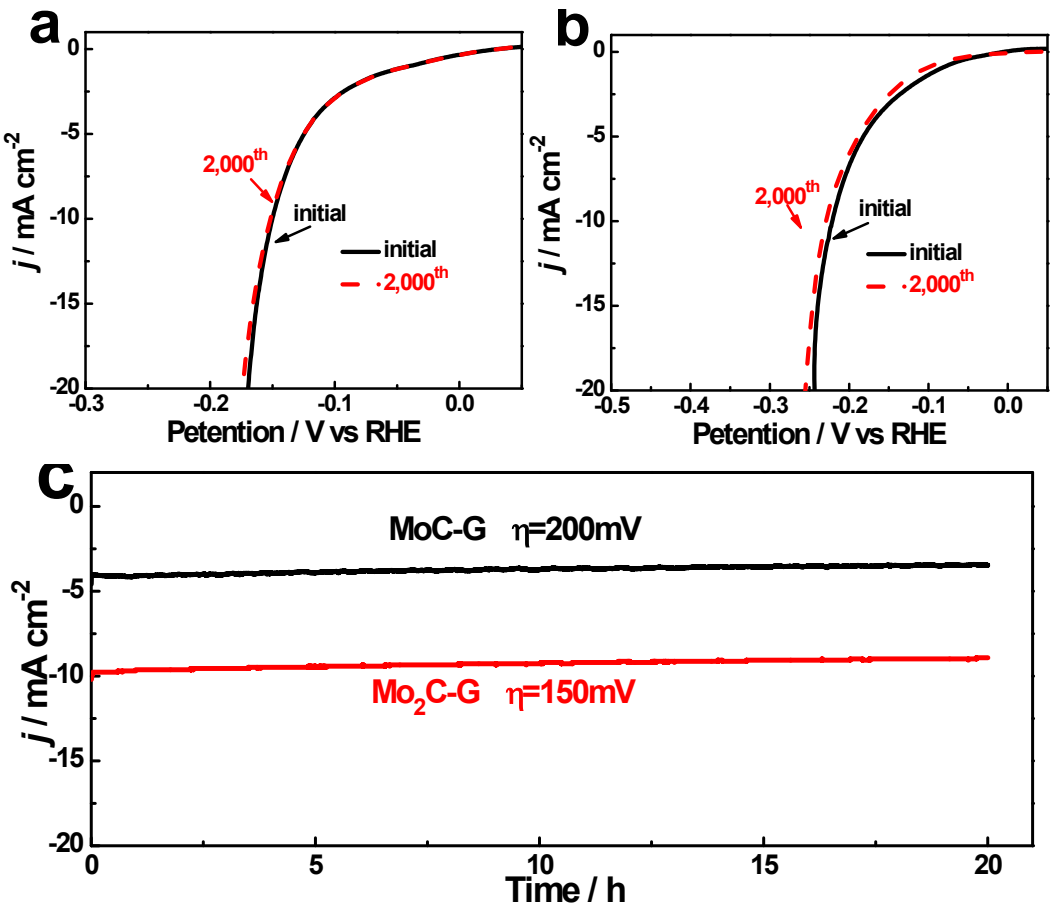

Figure S8 HER perfoemances of (a) MoC-G and (b) Mo_2C-G before and after a continuous potential swept for 2,000 cycles, (c) long-term stability of MoC-G and Mo_2C-G.

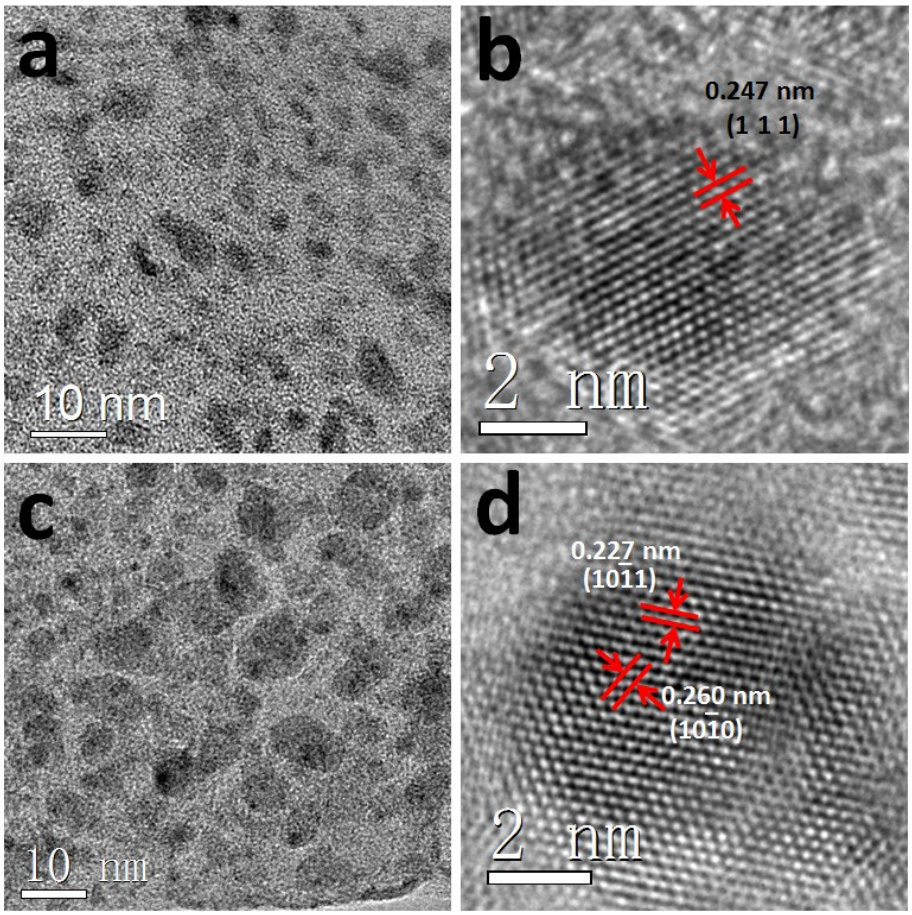

Figure S9 TEM images of MoC-G (a,b) and Mo_2C-G (c, d) after electrocatalytic durability testing

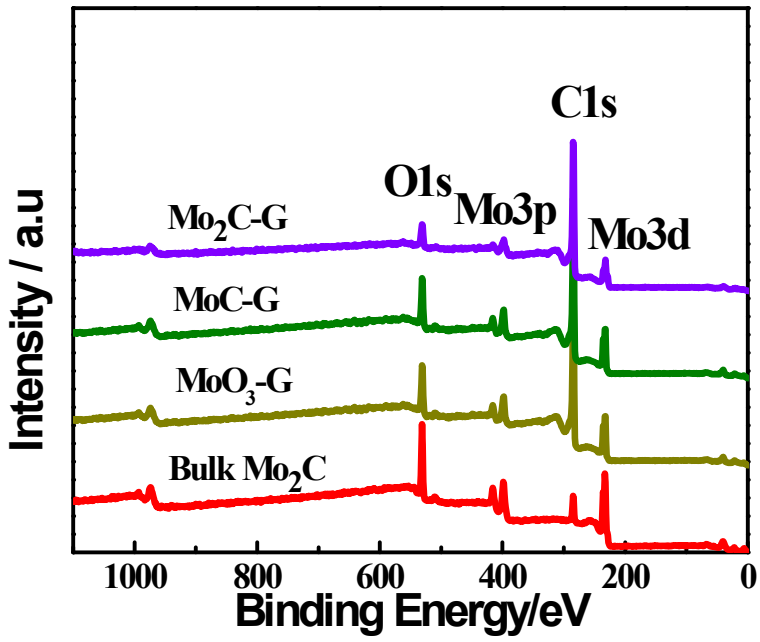

Figure S10 The survey XPS spectrum of MoO_3-G, bulk Mo_2C, MoC-G and Mo_2C-G.

Table S3 Structural parameters determined by the curve-fitting analysis of Mo *K*-Edge EXAFS for MoC-G, Mo_2C-G and bulk Mo_2C.

catalyst	Mo half step energy (eV)	R_{Mo-C}	N_{Mo-C}	R_{Mo-Mo}	N_{Mo-Mo}
MoC-G	20009.3	2.15	1.5± 0.29	3.04	1.6± 0.37
Mo_2C-G	20007.5	2.08	2.16± 0.55	2.98	8.4± 1.33
Bulk Mo_2C	20005.2	2.06	1.5 ± 0.46	2.97	4.9 ± 1.29

References

[1] L. Liao, S. Wang, J. Xiao, X. Bian, Y. Zhang, M. D. Scanlon, X. Hu, Y. Tang, B. Liu, H. H. Girault, Energy Environ. Sci. 7 (2014) 387-392.

[2] W. F. Chen, C. H. Wang, K. Sasaki, N. Marinkovic, W. Xu, J. T. Muckerman, Y. Zhu, R. R. Adzic, Energy Environ. Sci. 6 (2013) 943.

[3] D. H. Youn, S. Han, J. Y. Kim, J. Y. Kim, H. Park, S. H. Choi, J. S. Lee, ACS Nano 8 (2014) 5164-5173.

[4] W.-F. Chen, K. Sasaki, C. Ma, A. I. Frenkel, N. Marinkovic, J. T. Muckerman, Y. Zhu, R. R. Adzic, Angew. Chem. Int. Ed. 51 (2012) 6131-6135.

[5] P. Xiao, Y. Yan, X. Ge, Z. Liu, J.-Y. Wang, X. Wang, Appl. Catal., B : Environ. 154-155 (2014) 232-237.

[6] H. Vrubel, X. Hu, Angew. Chem. Int. Ed. 51 (2012) 12703-12706.

[7] Y. Li, H. Wang, L. Xie, Y. Liang, G. Hong, H. Dai, J. Am. Chem. Soc. 133 (2011) 7296-7299.

[8] J. Kibsgaard, T. F. Jaramillo, F. Besenbacher, Nat. Chem. 6 (2014) 248-253.

[9] F. H. Saadi, A. I. Carim, E. Verlage, J. C. Hemminger, N. S. Lewis, M. P. Soriaga, J. Phys. Chem. C 118 (2014) 29294-29300.

[10] W. Cui, Q. Liu, Z. Xing, A. M. Asiri, K. A. Alamry, X. Sun, Appl. Catal., B : Environ. 164 (2015) 144-150.

[11] D. Kong, H. Wang, Z. Lu, Y. Cui, J. Am. Chem. Soc. 136 (2014) 4897-4900.